npj | climate and atmospheric science

www.nature.com/npjclimatsci

ARTICLE OPEN

Check for updates

The parametric hurricane rainfall model with moisture and its application to climate change projections

Dasol Kim[1], Doo-Sun R. Park[2]✉, Chaehyeon C. Nam[3] and Michael M. Bell[3]

The parametric hurricane rainfall model (PHRaM), firstly introduced in 2007, has been widely used to forecast and quantify tropical-cyclone-induced rainfall (TC rainfall). The PHRaM is much more computationally efficient than global climate models, but PHRaM cannot be effectively utilized in the context of climate change because it does not have any parameters to capture the increase of tropospheric water vapor under the warming world. This study develops a new model that incorporates tropospheric water vapor to the PHRaM framework, named as the PHRaM with moisture (PHRaMM). The PHRaMM is trained to best fit the TC rainfall over the western North Pacific (WNP) unlike the PHRaM trained with the TCs over the continental US. The PHRaMM reliably simulates radial profile of TC rainfall and spatial distribution of accumulated rainfall during landfall in the present climate with the better prediction skills than existing statistical and operational numerical models. Using the PHRaMM, we evaluated the impacts of TC intensity and environmental moisture increase on TC rainfall change in a future climate. An increased TC intensity causes TC rainfall to increase in the inner-core region but to decrease in the outer region, whereas an increased environmental moisture causes the TC rainfall to increase over the entire TC area. According to the both effects of increased TC intensity and environmental moisture, the PHRaMM projected that the WNP TC rainfall could increase by 4.61–8.51% in the inner-core region and by 17.96–20.91% over the entire TC area under the 2-K warming scenario.

npj Climate and Atmospheric Science (2022)5:86 ; https://doi.org/10.1038/s41612-022-00308-9

INTRODUCTION

Tropical cyclones (TCs) often bring deadly disasters. Most of the fatalities and economic damages associated with TCs are water-related, such as surge and rainfall[1–5]. Rainfall-induced freshwater flooding is the most frequent occurring hazard compared to wind, tornado, or storm surge and accounts for about one-quarter of the deaths directly caused by hurricanes hitting the United States from 1963 to 2012[1]. The amount of rainfall produced by the TC was shown to be the most decisive factor in determining TC damages in South Korea[2–4]. By using a TC integrated assessment model, Bakkensen et al.[5] found that future losses by TC are significantly underestimated when not considering rainfall as one of the independent variables, highlighting the importance of considering TC rainfall in projecting future TC damages.

Damage from TC rainfall is likely to become only more severe over the next century as TC rainfall is expected to increase under global warming[6] as well as increasing population along the coast[5,7]. As air warms up, its capacity to hold water vapor increases at the Clausius-Clapeyron rate (~7% °C^{-1}), which can contribute to TC rainfall increase in future climate. However, according to climate models, TC rainfall might increase at a larger rate than the Clausius-Clapeyron rate. Knutson et al.[6] showed more than 20% of TC rainfall increase with 1.5–1.6 °C increase of sea surface temperature (SST) in the Western Pacific by late this century following Representative Concentration Pathway (RCP) 4.5 projection. The increased rainfall rate beyond the Clausius-Clapeyron rate is attributable to the ability of TCs to draw moisture from surrounding area (i.e., moisture convergence). Recent observational studies verified the increasing trend of TC rainfall—about 1.3% per year on average[8]. Both Tu et al.[9] and Guzman and Jiang[8] showed that the overall increase in TC rainfall is due to an increase in rain rate in the outer region, and TC rainfall has decreased significantly in the inner-core region; they attributed decreased rainfall in the inner-core region to increased atmospheric stability and explained increased rainfall in the outer region with increased SST and available moisture.

Since TC rainfall is closely related to TC intensity and environmental moisture, both TC intensity and environmental moisture should be considered for accurate TC rainfall prediction under global warming. The modeling study by Patricola and Wehner[10] compared TC rainfall under the pre-industrial, current, and the future climate, and their results showed that, from the pre-industrial to the current climate, TC rainfall increased over a very broad area without any noticeable change in TC intensity. However, in projections from the current to the future climate, TC rainfall increased by a larger magnitude with significant increase in TC intensity. Although not specified in their study, the increase in TC rainfall from the pre-industrial to the current climate should be related to an increase in environmental moisture, and that from the present to the future climate may be due to increases in both environmental moisture and TC intensity. Liu et al.[11] showed that the future increase in TC rainfall in total can be greater than the Clausius-Clapeyron rate, but the increase in TC rainfall at the same TC intensity follows the Clausius-Clapeyron rate (Fig. 2 in their study). They also suggested that the increase in TC rainfall greater than Clausius-Clapeyron rate was particularly evident within 100 km radii, because the increased TC intensity causes the environmental moisture to converge more strongly to the TC center. Their result indicates that TC rainfall can be greatly enhanced when the effects of increased intensity and environmental moisture are combined.

Most of the studies that have predicted TC rainfall in future climates have used numerical simulations. Global climate models have a horizontal grid spacing of tens to hundreds of kilometers in

[1]Department of Geography, University of Florida, Gainesville, FL, USA. [2]Department of Earth Science Education, Kyungpook National University, Daegu, South Korea. [3]Department of Atmospheric Science, Colorado State University, Fort Collins, CO, USA. ✉email: dsrpark@knu.ac.kr

general so that they cannot realistically simulate mesoscale TC structures. Mesoscale regional models can well capture such TC structures, however, they cannot cover the entire globe (table ES4 in Knutson et al.[12]) since they are computationally expensive. An alternative explored in the current study is the use of a parameterized model. Several parameterized models have been developed to model TC rainfall[13,14] and used for future TC rainfall studies[15]. The Rainfall Climatology & Persistence (R-CLIPER) model[16] is a parameterized model for TC rainfall, which had been used at the National Hurricane Center (NHC) experimentally for 2001–2003 and operationally since 2004. The R-CLIPER estimates TC rainfall as a function of TC intensity and the distance from the TC track using statistics derived from the Tropical Rainfall Measuring Mission (TRMM) rainfall data. Thus, R-CLIPER accounts for TC intensity, size, and translation speed but not shear asymmetry nor topography. Building on the R-CLIPER framework, the Parametric Hurricane Rainfall Model (PHRaM) was developed to include shear asymmetry and topography[17]. The PHRaM showed much improved performance than R-CLIPER mainly due to the newly added topographic impacts. However, the PHRaM still cannot be used to investigate TC rainfall in future climate because it does not account for environmental moisture.

In this paper, we introduce a newly developed PHRaM with moisture (PHRaMM). We added total column water (TCW) to the existing PHRaM framework, so that the PHRaMM can be used to assess TC rainfall under climate change. By adding moisture to the PHRaM framework, we can assess anthropogenic influences on TC rainfall while preserving the model's computational efficiency and accuracy. Also, the PHRaMM can linearly decompose the contribution of the TC intensity change and the environmental moisture change on the overall TC rainfall change.

RESULTS

Parametric Hurricane Rainfall Model with Moisture (PHRaMM)

The Parametric Hurricane Rainfall Model (PHRaM) originated from the rainfall climatology and persistence model (R-CLIPER)[16] which predicts radial distributions of TC rainfall using TC intensity (i.e., V_{max}). Lonfat et al.[17] developed the PHRaM as below (Eq. 1):

$$P_{PHRaM} = P_{sym} + P_{asym} + P_{topo} \quad (1)$$

where P_{PHRaM} indicates the total TC rainfall field predicted by the model, P_{sym} denotes symmetric rainfall predicted from the R-CLIPER component, and P_{asym} and P_{topo} indicate the newly added asymmetric rainfall induced by vertical wind shear and rainfall generated by topography, respectively.

The original version of PHRaM is not suitable for climate analysis as it does not take the environmental moisture into account to model TC rainfall. Therefore, we modified the PHRaM by adding terms of TCW to symmetric rainfall (P_{sym}) as shown in Eqs. 2–7. The newly developed model was named PHRaM with moisture (PHRaMM).

$$P_{sym}(r, V_{max}, TCW) = T_0 + (T_m - T_0)(r/R_m), (r < R_m) \quad (2)$$

$$P_{sym}(r, V_{max}, TCW) = T_m \times \exp[-(r - R_m)/R_e], (r > R_m) \quad (3)$$

$$T_0 = a_1 + b_1 V_{max} + c_1 TCW \quad (4)$$

$$T_m = a_2 + b_2 V_{max} + c_2 TCW \quad (5)$$

$$R_m = a_3 + b_3 V_{max} + c_3 TCW \quad (6)$$

$$R_e = a_4 + b_4 V_{max} + c_4 TCW \quad (7)$$

where P_{sym}, radial distributions of rainfall, is a function of the radius from the TC center (r), V_{max} is the maximum wind speed of TC, TCW is the total column water averaged within 500 km from the center of TC, T_0 is rain rate at the center of TC, T_m is the maximum rain rate in the radial profile of TC rainfall, R_m is the radius of maximum rain rate, and R_e is the e-folding radius of the maximum rain rate from the R_m. According to the Eqs. 2, 3, rainfall increases linearly with radius up to R_m and then decreases exponentially. The four rainfall parameters (i.e., T_0, T_m, R_m, and R_e) were calculated for a total of 7809 TC samples (an example of parameter calculation in Supplementary Fig. 1) and were used to construct linear regression models of Eqs. 4–7. Note that V_{max} and TCW were standardized using mean (30.63 m s^{-1} and 59.64 kg m^{-2}, respectively; Supplementary Fig. 2a) and standard deviation (10.11 m s^{-1} and 5.71 kg m^{-2}, respectively; Supplementary Fig. 2b) before constructing the regression models. We assume that the four rainfall parameters are related with TCW averaged within a radius of 500 km from the TC center as well as V_{max} (Eqs. 4–7). This assumption is reasonable because environmental moisture is a source of rainfall and can significantly affect rainfall structure of TCs such as intensity, areal extents, total amount, etc[18–22]. In particular, Jiang et al.[21] showed that the higher TCW within 500 km TC radius values are associated with higher TC volumetric rainfall. The linear regression coefficients of the four rainfall parameters are denoted by a, b, and c with numeric subscripts from 1 to 4. Note that the correlation coefficient between the V_{max} and TCW is 0.159. The collinearity between the independent variables can be measured using a variance inflation factor (VIF). Generally, a VIF > 5 indicates a problematically strong correlation between the independent variables, but the VIF is 1.03 in the PHRaMM.

Table 1 presents the regression coefficients for each rainfall parameter, and correlation coefficients between the observed and estimated values. The samples were divided into 10 subsets to validate the model using the leave-one-out cross validation (please see the details in the "Methods" section). The standard deviation of each coefficient for the 10 subsets is substantially smaller than the mean value, which means the model does not change significantly depending on the sample used. The partial regression and correlation coefficients are significant in 95% confidence level except for the regression coefficient of TCW for T_0. V_{max} has a positive relationship with T_0 and T_m and a negative

Table 1. The regression coefficients for the rainfall parameters to fit the Eqs. 4–7, and correlation coefficients between the observed and predicted values.

	Intercept	V_{max}	TCW	Corr. Coeff.
T_0 (mm h^{-1})	$a_1 = 5.53$ (0.07)	$b_1 = 0.85$ (0.06)	$c_1 = -0.06$ (0.05)	0.12 (0.009)
T_m (mm h^{-1})	$a_2 = 8.73$ (0.08)	$b_2 = 1.76$ (0.05)	$c_2 = 0.18$ (0.05)	0.26 (0.007)
R_m (km)	$a_3 = 75.2$ (0.71)	$b_3 = -9.0$ (0.48)	$c_3 = 3.8$ (0.54)	0.15 (0.008)
R_e (km)	$a_4 = 182.0$ (1.61)	$b_4 = -33.2$ (1.05)	$c_4 = 12.9$ (1.92)	0.19 (0.005)

Parenthesis indicates the standard deviation of each coefficient for the ten models according to the subsampling by the leave-one-out cross validation.

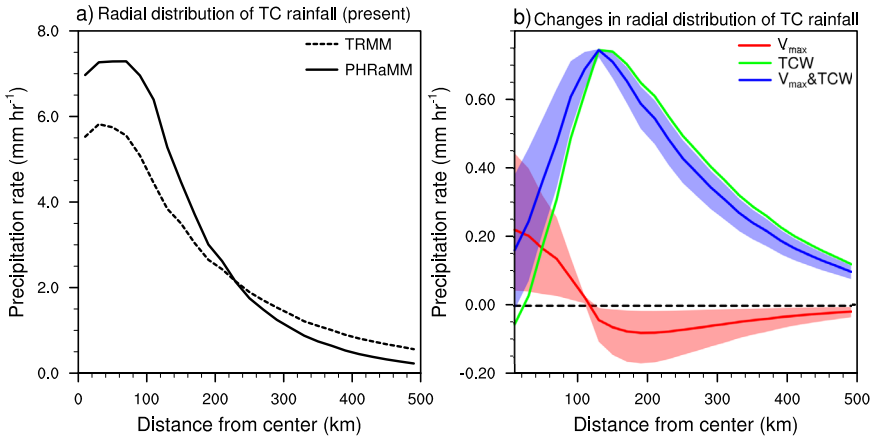

Fig. 1 Mean radial distribution of tropical cyclone (TC) rainfall in the present and future climate. a The TRMM (dashed line) and PHRaMM (solid line) for the present climate. **b** Future changes compared to the present climate according to the increases in the maximum wind speed (V_{max}) by 1–10% (red line and shading), increase in the total column water (TCW) by 14% (green line), and increase in both (blue line and shading). The red and blue lines indicate the results according to the median value of V_{max} increases (+5%), and shadings present the ranges of change based on the ranges of V_{max} increases (+1–10%).

relationship with R_m and R_e, which is consistent with the results of the original PHRaM and R-CLIPER (Table 2 in Tuleya et al.[16]). The magnitudes of regression coefficients of the PHRaMM may be different from those of the original model because V_{max} in the original model is normalized using arbitrary values (i.e., 33 and 35 knots) instead of the mean and standard deviation of the TC observation data. The regression coefficients of TCW for T_0, and T_m are about 10 times smaller than those of V_{max}, whereas the coefficients of TCW for R_m and R_e is comparable to those of V_{max} (i.e., 3.8 vs. −9.0 and 12.9 vs. −33.2, respectively). These results suggest that TCW mainly modulates the spatial size of TC rainfall by changing R_m and R_e, but has no significant effect on intensity of rainfall near the inner-core region.

The asymmetric rainfall component (P_{asym}) associated with the vertical wind shear in the PHRaMM is expressed by Eq. 8, which is the same as that in the original PHRaM.

$$P_{asym}(r,\theta) = \sum A_i(r)cos(i\theta) + \sum B_i(r)sin(i\theta) \quad (8)$$

Where P_{asym} is a function of r and the azimuthal angle from the vertical wind shear vector (θ). A_i and B_i are the Fourier coefficients of rainfall in azimuthal direction for the wavenumber i (only the wavenumbers 1 and 2 are considered here). As the original PHRaM was developed for the North Atlantic TCs, we newly calculated the parameters in Eq. 8 for the rainfall asymmetry associated with vertical wind shear for the western North Pacific TCs. As in the original PHRaM, the Fourier coefficients were parameterized for three shear categories and three TC intensity classes (i.e., 9 groups in total). The categories for vertical wind shear are weak shear (<5 m s^{-1}), medium shear (5–10 m s^{-1}), and strong shear (>10 m s^{-1}), respectively. The three TC intensity classes consist of tropical storm (TS), Saffir–Simpson categories 1 to 2, and Saffir–Simpson categories 3 to 5. Supplementary Figs. 3–5 show the radial distributions of Fourier coefficients for the 9 groups. Similar to the original PHRaM, B_1 has a positive value with the largest magnitude up to 100% and the remaining coefficients have negative values ranging from −40% to 0%. The peaks of the coefficients appeared in the 100–400 km radius, which is also consistent with the results of the original model. A positive B_1 means a dipole structure of enhanced rainfall on the downshear side and decreased rainfall in the upshear side, and a negative A_1 means increased rainfall on the shear-left side and decreased rainfall on the shear-right side. That is, rainfall is strengthened and weakened in downshear-left and upshear-right sides, respectively, which is consistent with the previous studies[19,23–28].

The topographic rainfall component (P_{topo}) is represented by Eqs. 9, 10.

$$P_{topo} = [L/(1000\,\mathrm{m})] \times [P_{sym} + P_{asym}], (L > 0) \quad (9)$$

$$P_{topo} = [0.2 \times L/(1000\,\mathrm{m})] \times [P_{sym} + P_{asym}], (L < 0) \quad (10)$$

where L is the lift of air parcel forced by topography during one time step (i.e., 1 h) in meter. L can be expressed as $w_{topo} \times (3600\,\mathrm{s}) = \vec{\mathbf{V}}_s \cdot \nabla h_s \times (3600\,\mathrm{s})$, where w_{topo} is vertical velocity induced by topography, $\vec{\mathbf{V}}_s$ is horizontal winds at the surface, and h_s is surface elevation. L is divided by 1000 m in this study to adjust the topographic effect. The downslope effect ($L < 0$) is 5 times smaller than the upslope effect ($L > 0$), which is the same as that of Lonfat et al.[17]. Although this method is empirical, it effectively captures rainfall induced by topography.

The PHRaMM was evaluated by comparing the observations and simulations of TC rainfall in terms of the radial distribution of rainfall and spatial distribution of accumulated rainfall during landfall for the entire analysis period. Figure 1a shows the mean radial distributions of TC rainfall obtained from the TRMM (dashed line) and PHRaMM (solid line) for the present climate. The radial distribution of rainfall simulated by the model closely resembles that of the observation. The difference of maximum precipitation between the model and observation is 1.47 mm h^{-1}. The root mean squared error for the radial profile of rainfall is only 0.38 mm h^{-1}. These biases of the PHRaMM are noticeably smaller than those of other numerical and statistical models[29,30]. In addition, variations in the radial profile of TC rainfall according to the V_{max} and TCW was examined (Supplementary Fig. 6). The maximum precipitation significantly varies according to the V_{max}, which can be consistently found in the observation and simulation (Supplementary Fig. 6a). On the other hand, TC rainfall clearly expands in the radial direction with the increasing TCW both in the observation and model (Supplementary Fig. 6b), although the magnitude of variation in the model is less than that in observations (about 60%).

Figure 2a, b presents the climatology of annual accumulated rainfall in the observation and simulation for the 288 TC landfall cases. The spatial distribution of accumulated rainfall during the TC landfall is reliably simulated both in pattern and magnitude. The pattern correlation between the observation and simulation is 0.959 for only the grid points with accumulated rainfall greater than 0 mm and the root mean squared error of the model is 22.30 mm. Figure 3 presents the pattern correlation and normalized standard deviation between the observed and simulated

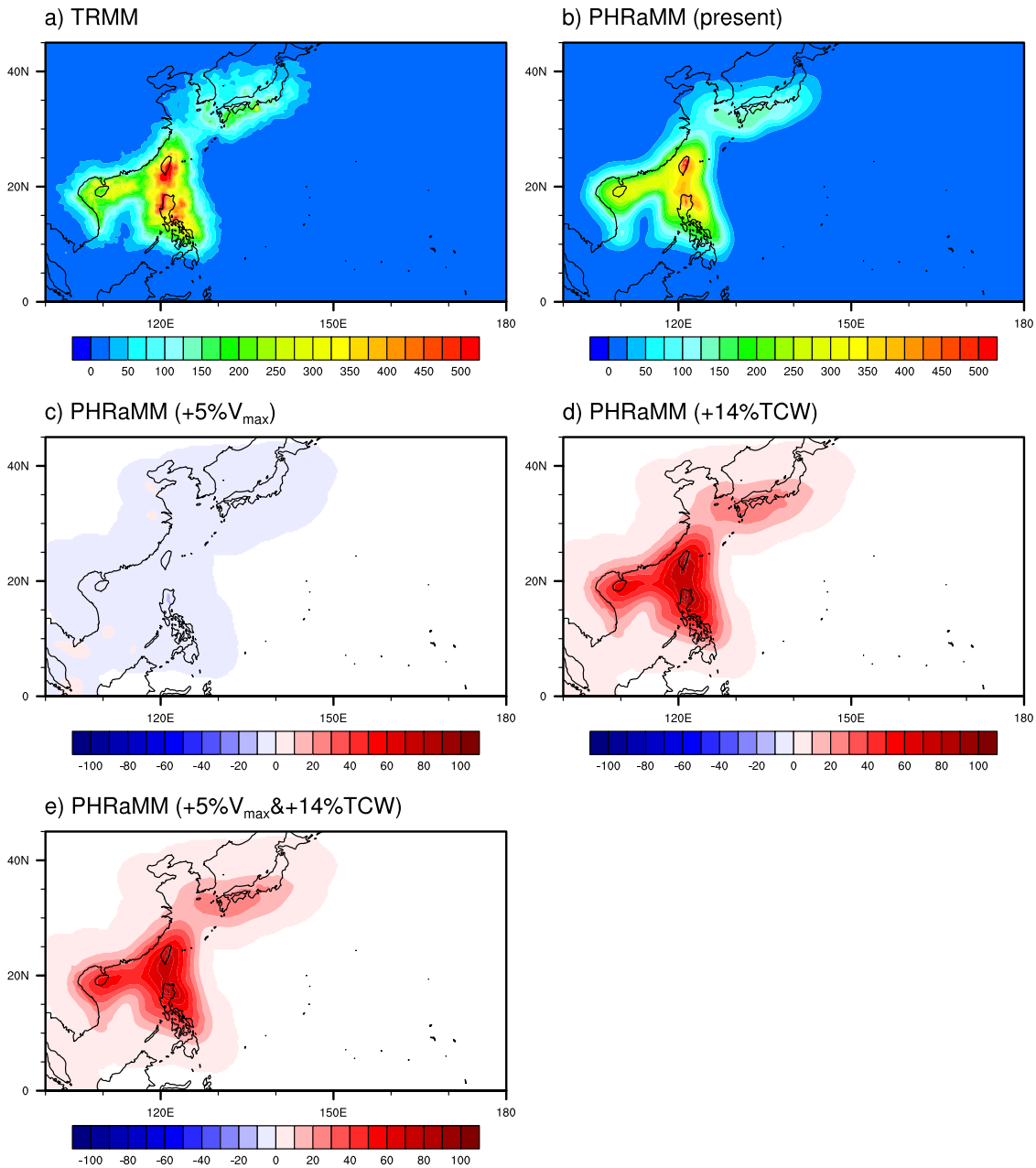

Fig. 2 Annual mean accumulated TC rainfall during the landfall period in the present climate and future climate. a The TRMM and **b** PHRaMM for the present climate. Future changes compared to the present climate according to the **c** increase in V_{max} by 5%, **d** increase in TCW by 14%, and **e** increase in both.

spatial distribution of accumulated rainfall for each landfall case. The normalized standard deviation is the ratio of the standard deviation of rainfall simulated by the PHRaMM to that in the TRMM. If the normalized standard deviation is close to 1, it means that the model successfully simulated the magnitude of the rainfall variability in the observation. The pattern correlation and normalized standard deviation generally appear in the range of 0.7–0.9 and 0.5–1.5, respectively. The mean values of pattern correlation and normalized standard deviation are 0.760 and 0.878, respectively (red star in Fig. 2). Previous statistical models that predict TC rainfall over the North Atlantic have the pattern correlation values with observations ranging from 0.380 to 0.467[31]. The pattern correlation of operational numerical models for North Atlantic TC rainfall is in the range of 0.50 to 0.68[32]. Therefore, our model has better performance than the existing statistical and operational numerical models in predicting spatial distribution of TC rainfall. The reason that the PHRaMM has better performance than other statistical models over the North Atlantic is probably because the PHRaMM not only includes rainfall asymmetry and topographical effects, but also uses much greater number of samples over the WNP for model development. Note that the annual number of TCs in the WNP is about two times higher than that in the North Atlantic.

Changes in TC rainfall under global warming

Changes in TC rainfall under global warming were estimated by applying future projections of V_{max} and TCW to the PHRaMM. The projected V_{max} and TCW in this study were based on the results of Knutson et al.[12]. Knutson et al.[12] suggested that V_{max} can increase by

Table 2. Changes in rainfall in the inner-core (within 100 km radius) and the total area (within 500 km radius) according to the 1–10% increment of V_{max}, 14% increment of TCW, and both.

	V_{max}	TCW	V_{max} and TCW
Inner-core	[0.027, 0.247] mm h^{-1} ([0.39, 3.63] %)	0.283 mm h^{-1} (4.15%)	[0.314, 0.580] mm h^{-1} ([4.61, 8.51] %)
Total	[−0.052, −0.005] mm h^{-1} ([−3.59, −0.33] %)	0.309 mm h^{-1} (21.19%)	[0.262, 0.305] mm h^{-1} ([17.96, 20.91] %)

Values are the averages of the total 288 TC landfall cases. Square brackets present range of values (i.e., [min, max]). Parentheses indicate the rate of change in percentage.

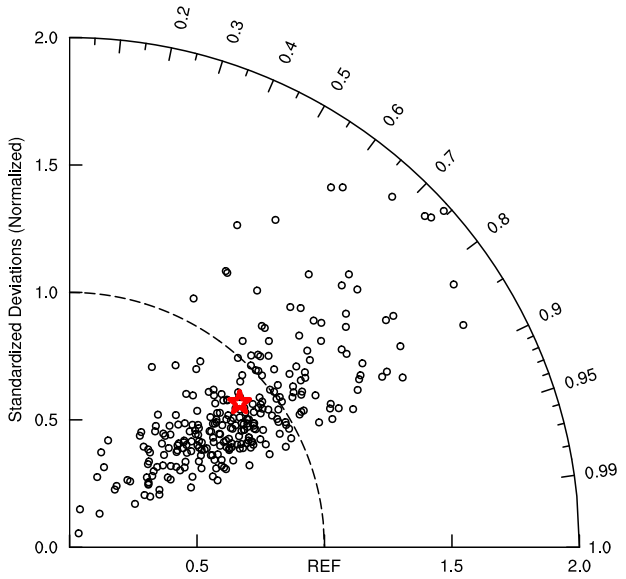

Fig. 3 Taylor diagram of the pattern correlation and normalized standard deviation for accumulated rainfall during each TC landfall from TRMM observation and PHRaMM prediction. The radial direction represents the normalized standard deviation, and the azimuthal direction represents the pattern correlation coefficient. The normalized standard deviation is defined as the ratio of the standard deviation of precipitation simulated by the PHRaMM to that in the TRMM. Black circles represent individual TC cases and red star denotes the average value of the total 288 landfall cases, respectively.

1–10% (median: 5%) by reviewing multiple global climate model simulations in previous studies. Most of the projections in the previous studies are based on the future climate scenarios in the Coupled Model Intercomparison Projects (CMIPs) such as A1B, RCPs scenarios. We believe the range of change in V_{max} suggested by Knutson et al.[12] is the most plausible because they investigated most of the previous studies available in the last 20 years. In addition, the TCW was projected to increase by 14% as the average value of the predicted temperature increase in the most of previous studies is 2-K. Therefore, we examined the changes in TC rainfall by applying the V_{max} increase in the range of 1 to 10% at 1% intervals and the TCW increase by 14%.

Figure 1b presents the changes in the radial distribution of TC rainfall compared to the present climate. According to the V_{max} increase, the rainfall in the inner-core (within 100 km radius) increases, while that in the outer region decreases (red line and shading in Fig. 1b). This feature can be clearly seen in Table 2 which presents TC rainfall changes averaged within 100 km and 500 km radius from the TC center, respectively (i.e., inner-core and total area, respectively). The inner-core rainfall increased in the range from 0.39% to 3.63% according to the increasing V_{max} by 1–10%, but the rainfall in total area decreased in the range from −3.59% to −0.33%. This implies that TC intensity acts to spatially redistribute TC rainfall. Our hypothesis is that as stronger V_{max} accompanies stronger convergence near the TC center, moisture concentrates in the inner-core region and thins out in the outer region given a constant environmental moisture, which promotes rainfall focused in the inner-core region. In many observational studies, the positive relationship between TC rainfall and V_{max} is robust only near the center within 300 km, and a negative relationship between them appears in the outer region[20,27,28,31]. Similarly, the future TC rainfall increase projected from the Global Climate Models (GCMs) is particularly evident within 100 km from TC center (table ES4 in Knutson et al.[12]), which can be explained by the stronger convergence in the inner-core region[11].

On the other hand, rainfall increases in most radii according to the increasing TCW (green line in Fig. 1b). Particularly, the increase in rainfall is maximized near 140 km radius and decreased more gradually in the outer regions than in the inner-core. The average rainfall changes in the inner-core and total area are 4.15 and 21.29%, respectively (Table 2). Thus, the rainfall changes in percentage are most predominant in the outer region. This is because the outer region has relatively less rainfall on average but occupies a larger area compared to the inner-core. In addition, the different sensitivity of rainfall to environmental conditions in the inner-core and outer region can be related to the thermodynamic structure of TCs. The circulation of a TC is mostly accounted by the primary circulation which is a horizontal and cyclonic circulation[33]. In the boundary layer, the gradient wind balance of the primary circulation is broken by the friction, which causes a strong convergence to the center of TC[34–36]. This strong convergence not only induces an intense convection, but also causes the humidity near the center to be higher than outside. Therefore, the rainfall in the inner-core region may not change sensitively to the changes in environmental humidity due to the existing strong convection and sufficiently high humidity in there, whereas even a small change in humidity by large-scale environments can have a large effect on the rainfall in the outer region.

The changes in rainfall by the increases in both V_{max} and TCW (blue line and shading in Fig. 1b) are similar to those by the increase in TCW only, but rainfall relatively increases more in the inner-core and less in the outer region. This result is because both V_{max} and TCW promote rainfall in the inner-core, whereas the effects of the two are opposite to each other in the outer region. The positive TCW effect on outer region is so large that it can overcompensate the negative V_{max} effect. Therefore, the inner-core rainfall is simulated to increase in the range of 4.61–8.51% and the total rainfall is projected to increase in the range of 17.96–20.91%, respectively (Table 2).

The changes in spatial distributions of annual accumulated rainfall during landfall according to the increasing V_{max} by 5% (the median value of its change) and TCW by 14% are provided in Fig. 2c–e. The accumulated rainfall slightly decreased (<10 mm) in most regions due to the V_{max} increase (Fig. 2c). On the other hand, according to the TCW increase, the accumulated rainfall greatly increased by more than 20 mm in most regions, and by more than 100 mm in Taiwan and the Philippines (Fig. 2d). Finally, the changes in accumulated rainfall associated with both increase in the V_{max} and TCW (Fig. 2e) can be mostly accounted by those with

the increase in the TCW only. According to the previous studies, there is a larger uncertainty in TC intensity projection for the future (e.g., 1–10%), but it is a robust projection that environmental moisture will increase under global warming. Our results imply that, even if the future climate does not produce stronger TCs, the increased moisture alone can produce much heavier TC rainfall.

DISCUSSION

In this study, we introduce the newly developed PHRaMM, following the basic structure of the original PHRaM. The key difference of the PHRaMM from the PHRaM is that the PHRaMM can capture changes in tropospheric water in the surrounding environment of the TCs, so that it can be applied to project TC rainfall in the future climate. Some parameters of the PHRaMM (e.g., the Fourier coefficients for the rainfall asymmetry) were newly calculated with the western North Pacific TC samples since the original model parameters were optimized for the North Atlantic TCs. The PHRaMM for the western North Pacific was evaluated by using a total of 288 TC landfall cases. The radial profile and spatial distribution of accumulated rainfall during the landfall were reasonably simulated by the PHRaMM. The performance of the PHRaMM is better than existing statistical and operational numerical models in terms of pattern correlation and normalized standard deviation for the accumulated rainfall during landfall with the mean values of 0.760 and 0.878, respectively.

Using the PHRaMM, we investigated future TC rainfall changes under the global warming, in which V_{max} and TCW increase by 1–10% and 14%, respectively[12]. According to our results, increased V_{max} yields increased TC rainfall in the inner-core region and slightly decreased TC rainfall in the outer region, whereas increased TCW enhances TC rainfall over the broad TC area. Both increased V_{max} and TCW together produce TC rainfall increase of 4.61–8.51% in the inner-core and 17.96–20.91% in total area. The greater increase in rainfall at the outer region than at the inner-core also has been reported in several observational and numerical model studies[8,9,37]. Particularly, according to the results of Wright et al.[37], the average increase in rainfall at the outer region was about twice that at the inner-core (Table 6 in their study). In short, increasing environmental moisture amplifies the TC rainfall universally over a broad TC-affected area but increasing TC intensity acts to redistribute the moisture resulting rainfall enhanced in the inner-core region and suppressed over the outer region. These relationships we found among TC rainfall, TC intensity, and environmental moisture are consistent with the results alluded by previous studies using numerical dynamic models[10,11].

The PHRaMM has some intrinsic limitations as a statistical model such that it does not explicitly simulate complex and non-linear mesoscale dynamics. As Table 1 and Fig. 3 show, the PHRaMM cannot explain all the variance of the TC rainfall observations. However, we believe that the PHRaMM is a useful and reliable tool for future TC rainfall projection in a climatological perspective. First, our results of the increase in the total TC rainfall predicted by the PHRaMM (i.e., 17.96–20.91% increase) are consistent with the results of previous studies (e.g., 6–22% in Knutson et al.[12]). Second, the PHRaMM requires less computational resources compared to the global convection-permitting dynamic models. Lastly, the PHRaMM can linearly quantify the effects of TC intensity and environmental moisture on TC rainfall changes separately. Hence, we propose the PHRaMM can be an intermediate method to examine TC rainfall until we easily get the computing power to run convection permitting global climate models that can simulate mesoscale TC dynamics in a future climate.

METHODS

Data

Tropical cyclone (TC) information including the location of the TC center in latitude and longitude, 10-min averaged maximum sustained wind speed (V_{max}), and designation of TC in 6-hour intervals for the western North Pacific (WNP) was obtained from the best-track data of the Regional Specialized Meteorological Center's (RSMC) Tokyo Typhoon Center. Using the designation information of the TCs, extratropical cyclones and tropical depressions were excluded in this study. The total number of TCs in the WNP during the analysis period (1998–2014) is 391, and the number of landfall TCs is 288. The landfall of TC was defined when the center of TC located within 300 km from the coastline (gray area in Supplementary Fig. 7). This definition has been widely used in other studies because the socioeconomic impacts of TCs on the coastal countries can appear even before the center of the TC goes into the landmass[3,4,38]. For model development and evaluation, rainfall fields within 1000 km from the center of TC were collected from the Tropical Rainfall Measuring Mission (TRMM) 3B42 precipitation data[39]. The TRMM 3B42 data cover 50°S–50°N with spatial and temporal resolutions of 0.25° and 3-hr. A total of 7809 samples of TC rainfall fields from the 391 TCs were collected based on the best-track data at 6-h intervals over the entire period. The fifth-generation reanalysis data from the European Centre for Medium-Range Weather Forecasts (ERA5)[40], were used to examine vertical wind shear (VWS), total column water (TCW), and orography around a TC. The VWS is defined as the difference of winds between 200 and 850 hPa levels and is averaged over an annular region of 200–800 km around the TC center. The TCW from the surface to the top of the atmosphere was averaged over the area within 500 km from the TC center. Two-dimensional orography data were calculated by dividing the surface geopotential from the ERA5 by the Earth's gravitational acceleration (i.e., $g = 9.80665\ m\ s^{-2}$). The spatial and temporal resolutions of ERA5 reanalysis data are 0.25° and 1-hr, respectively.

Leave-one-out cross-validation method

The PHRaMM has been validated using the leave-one-out cross validation. The samples were divided into 10 subsets (9 sets of each 781 samples and 1 set of 780 samples; total 7809 samples). To validate TC rainfall for each subset, a model was developed using the remaining samples. For example, for the prediction of the first 781 samples, the model was developed with the remaining 7028 samples. Therefore, 10 models were developed in this study, and the mean and standard deviation of their parameters are presented in Table 1 and Supplementary Figs. 3–5.

DATA AVAILABILITY

The best-track data from the RSMC's Tokyo Typhoon Center are available at https://www.jma.go.jp/jma/jma-eng/jma-center/rsmc-hp-pub-eg/besttrack.html. The TRMM 3B42 data can be downloaded at https://disc2.gesdisc.eosdis.nasa.gov/opendap/TRMM_L3/TRMM_3B42.7/. The ERA-5 reanalysis data can be assessed from https://cds.climate.copernicus.eu/#!/search?text=ERA5&type=dataset. The parameters and output of the PHRaMM model are available from the corresponding author upon reasonable request.

CODE AVAILABILITY

The source codes for the PHRaMM model are available from the corresponding author upon reasonable request.

Received: 16 March 2022; Accepted: 12 October 2022;
Published online: 04 November 2022

REFERENCES

1. Rappaport, E. N. Fatalities in the United States from Atlantic tropical cyclones: new data and interpretation. *Bull. Am. Meteorol. Soc.* **95**, 341–346 (2014).
2. Park, D.-S. R., Ho, C.-H., Nam, C. C. & Kim, H.-S. Evidence of reduced vulnerability to tropical cyclones in the Republic of Korea. *Environ. Res. Lett.* **10**, 054003 (2015).

3. Park, D.-S. R., Ho, C.-H., Kim, J., Kang, K. & Nam, C. C. Highlighting socioeconomic damages caused by weakened tropical cyclones in the Republic of Korea. *Nat. Hazards* **82**, 1301–1315 (2016).
4. Nam, C. C., Park, D.-S. R., Ho, C.-H. & Chen, D. Dependency of tropical cyclone risk on track in South Korea. *Nat. Hazards Earth Syst. Sci.* **18**, 3225–3234 (2018).
5. Bakkensen, L. A., Park, D.-S. R. & Sarkar, R. S. R. Climate costs of tropical cyclone losses also depend on rain. *Environ. Res. Lett.* **13**, 074034 (2018).
6. Knutson, T. R. et al. Global projections of intense tropical cyclone activity for the late twenty-first century from dynamical downscaling of CMIP5/RCP4.5 scenarios. *J. Clim.* **28**, 7203–7224 (2015).
7. Mendelsohn, R., Emanuel, K., Chonabayashi, S. & Bakkensen, L. The impact of climate change on global tropical cyclone damage. *Nat. Clim. Change* **2**, 205–209 (2012).
8. Guzman, O. & Jiang, H. Global increase in tropical cyclone rain rate. *Nat. Commun.* **12**, 5344 (2021).
9. Tu, S. et al. Recent global decrease in the inner-core rain rate of tropical cyclones. *Nat. Commun.* **12**, 1948 (2021).
10. Patricola, C. M. & Wehner, M. F. Anthropogenic influences on major tropical cyclone events. *Nature* **563**, 339–346 (2018).
11. Liu, M., Vecchi, G. A., Smith, J. A. & Knutson, T. R. Causes of large projected increases in hurricane precipitation rates with global warming. *NPJ Clim. Atmos. Sci.* **2**, 38 (2019).
12. Knutson, T. et al. Tropical cyclones and climate change assessment: Part II: Projected Response to Anthropogenic Warming. *Bull. Am. Meteorol. Soc.* **101**, E303–E322 (2020).
13. Lu, P., Lin, N., Emanuel, K., Chavas, D. & Smith, J. Assessing hurricane rainfall mechanisms using a physics-based model: Hurricanes Isabel (2003) and Irene (2011). *J. Atmos. Sci.* **75**, 2337–2358 (2018).
14. Langousis, A. & Veneziano, D. Theoretical model of rainfall in tropical cyclones for the assessment of long-term risk. *J. Geophys. Res. Atmospheres* **114**, D02106 (2009).
15. Emanuel, K. Assessing the present and future probability of Hurricane Harvey's rainfall. *Proc. Natl Acad. Sci. USA* **114**, 12681–12684 (2017).
16. Tuleya, R. E., DeMaria, M. & Kuligowski, R. J. Evaluation of GFDL and Simple Statistical Model Rainfall Forecasts for U.S. Landfalling Tropical Storms. *Weather Forecast* **22**, 56–70 (2007).
17. Lonfat, M., Rogers, R., Marchok, T. & Marks, F. D. A parametric model for predicting hurricane rainfall. *Mon. Wea. Rev.* **135**, 3086–3097 (2007).
18. Matyas, C. J. Processes influencing rain-field growth and decay after tropical cyclone landfall in the United States. *J. Appl. Meteor. Climatol.* **52**, 1085–1096 (2013).
19. Matyas, C. J. Associations between the size of hurricane rain fields at landfall and their surrounding environments. *Meteor. Atmos. Phys.* **106**, 135–148 (2010).
20. Kim, D., Ho, C.-H., Murakami, H. & Park, D.-S. R. Assessing the influence of large-scale environmental conditions on the rainfall structure of atlantic tropical cyclones: an observational study. *J. Clim.* **34**, 2093–2106 (2021).
21. Jiang, H., Halverson, J. B. & Zipser, E. J. Influence of environmental moisture on TRMM-derived tropical cyclone precipitation over land and ocean. *Geophys. Res. Lett.* **35**, L17806 (2008).
22. Hill, K. A. & Lackmann, G. M. Influence of environmental humidity on tropical cyclone size. *Mon. Wea. Rev.* **137**, 3294–3315 (2009).
23. Chen, S. S., Knaff, J. A. & Marks, F. D. Jr. Effects of vertical wind shear and storm motion on tropical cyclone rainfall asymmetries deduced from TRMM. *Mon. Wea. Rev.* **134**, 3190–3208 (2006).
24. Corbosiero, K. L. & Molinari, J. The relationship between storm motion, vertical wind shear, and convective asymmetries in tropical cyclones. *J. Atmos. Sci.* **60**, 366–376 (2003).
25. Frank, W. M. & Ritchie, E. A. Effects of environmental flow upon tropical cyclone structure. *Mon. Wea. Rev.* **127**, 2044–2061 (1999).
26. Frank, W. M. & Ritchie, E. A. Effects of vertical wind shear on the intensity and structure of numerically simulated hurricanes. *Mon. Wea. Rev.* **129**, 2249–2269 (2001).
27. Kim, D., Ho, C.-H., Park, D.-S. R., Chan, J. C. L. & Jung, Y. The relationship between tropical cyclone rainfall area and environmental conditions over the subtropical oceans. *J. Clim.* **31**, 4605–4616 (2018).
28. Kim, D., Ho, C. H., Park, D. R. & Kim, J. Influence of vertical wind shear on wind- and rainfall areas of tropical cyclones making landfall over South Korea. *PLoS ONE* **14**, e0209885 (2019).
29. Zhang, W. et al. Tropical cyclone precipitation in the HighResMIP atmosphere-only experiments of the PRIMAVERA Project. *Clim. Dyn.* **57**, 253–273 (2021).
30. Xi, D., Lin, N. & Smith, J. Evaluation of a physics-based tropical cyclone rainfall model for risk assessment. *J. Hydrometeor* **21**, 2197–2218 (2020).
31. Brackins, J. T. & Kalyanapu, A. J. Evaluation of parametric precipitation models in reproducing tropical cyclone rainfall patterns. *J. Hydrol.* **580**, 124255 (2020).
32. Marchok, T., Rogers, R. & Tuleya, R. Validation schemes for tropical cyclone quantitative precipitation forecasts: evaluation of operational models for U.S. landfalling cases. *Weather Forecast* **22**, 726–746 (2007).
33. Willoughby, H. E. Gradient balance in tropical cyclones. *J. Atmos. Sci.* **47**, 265–274 (1990).
34. Montgomery, M. T. & Smith, R. K. Recent developments in the fluid dynamics of tropical cyclones. *Annu. Rev. Fluid Mech.* **49**, 541–574 (2017).
35. Smith, R. K. & Montgomery, M. T. Hurricane boundary-layer theory. *Quart. J. Roy. Meteor. Soc.* **136**, 1665–1670 (2010).
36. Smith, R. K., Montgomery, M. T. & Van Sang, N. Tropical cyclone spin-up revisited. *Quart. J. Roy. Meteor. Soc.* **135**, 1321–1335 (2009).
37. Wright, D. B., Knutson, T. R. & Smith, J. A. Regional climate model projections of rainfall from U.S. landfalling tropical cyclones. *Clim. Dyn.* **45**, 3365–3379 (2015).
38. Park, D.-S. R. et al. A performance evaluation of potential intensity over the tropical cyclone passage to South Korea simulated by CMIP5 and CMIP6 models. *Atmosphere* **12**, 1214 (2021).
39. Huffman, G. J. et al. The TRMM multisatellite precipitation analysis (TMPA): quasi-global, multiyear, combined-sensor precipitation estimates at fine scales. *J. Hydrometeor* **8**, 38–55 (2007).
40. Hersbach, H. et al. The ERA5 global reanalysis. *Quart. J. Roy. Meteor. Soc.* **146**, 1999–2049 (2020).

ACKNOWLEDGEMENTS

This study was supported by the National Research Foundation of the Korean government (NRF-2019R1I1A3A01058100, NRF-2020R1A4A3079510, and NRF-2021R1A6A3A14044418), Korea Meteorological Administration Research and Development Program (KMI2022-01312), and the U.S. National Science Foundation award AGS-1854607. The authors thank Frank Marks for providing the source code of PHRaM. We also thank the three anonymous reviewers for their valuable comments to improve this study.

AUTHOR CONTRIBUTIONS

C.C.N. proposed the original idea, and all authors contributed to improve it. D.K., D.S.R.P., and C.C.N. wrote the draft, and all authors contributed to revise it. D.K. carried out all the calculations.

COMPETING INTERESTS

The authors declare no competing interests.

ADDITIONAL INFORMATION

Supplementary information The online version contains supplementary material available at https://doi.org/10.1038/s41612-022-00308-9.

Correspondence and requests for materials should be addressed to Doo-Sun R. Park.

Reprints and permission information is available at http://www.nature.com/reprints

Publisher's note Springer Nature remains neutral with regard to jurisdictional claims in published maps and institutional affiliations.